

Fast myocardial T_1 mapping using cardiac motion correction

Kirsten M. Becker¹  | Edyta Blaszczyk^{2,3,4} | Stephanie Funk^{2,3,4} | André Nuesslein¹ |
Jeanette Schulz-Menger^{2,3,4} | Tobias Schaeffter^{1,5} | Christoph Kolbitsch^{1,5} 

¹Physikalisch-Technische Bundesanstalt (PTB), Braunschweig and Berlin, Germany

²Charité Medical Faculty University Medicine, Berlin, Germany

³Working Group on Cardiovascular Magnetic Resonance, Experimental and Clinical Research Center (ECRC), Charité Humboldt University Berlin, DZHK partner site Berlin, Berlin, Germany

⁴Department of Cardiology and Nephrology, HELIOS Klinikum Berlin Buch, Berlin, Germany

⁵School of Biomedical Engineering and Imaging Sciences, King's College London, London, United Kingdom

Correspondence

Kirsten Becker, Physikalisch-Technische Bundesanstalt (PTB), Braunschweig and Berlin, Germany, Abbestr. 2-12, 10587 Berlin, Germany.
Email: kirsten.becker@ptb.de

Funding information

German Research Foundation (grants DFG-RTG2260 BioQic and DFG-CRC1340 Matrix in Vision).

Purpose: To improve the efficiency of native and postcontrast high-resolution cardiac T_1 mapping by utilizing cardiac motion correction.

Methods: Common cardiac T_1 mapping techniques only acquire data in a small part of the cardiac cycle, leading to inefficient data sampling. Here, we present an approach in which 80% of each cardiac cycle is used for T_1 mapping by integration of cardiac motion correction. Golden angle radial data was acquired continuously for 8 s with in-plane resolution of $1.3 \times 1.3 \text{ mm}^2$. Cine images were reconstructed for nonrigid cardiac motion estimation. Images at different TIs were reconstructed from the same data, and motion correction was performed prior to T_1 mapping. Native T_1 mapping was evaluated in healthy subjects. Furthermore, the technique was applied for postcontrast T_1 mapping in 5 patients with suspected fibrosis.

Results: Cine images with high contrast were obtained, leading to robust cardiac motion estimation. Motion-corrected T_1 maps showed myocardial T_1 times similar to cardiac-triggered T_1 maps obtained from the same data ($1288 \pm 49 \text{ ms}$ and $1259 \pm 55 \text{ ms}$, respectively) but with a 34% improved precision (spatial variation: $57.0 \pm 12.5 \text{ ms}$ and $94.8 \pm 15.4 \text{ ms}$, respectively, $P < 0.0001$) due to the increased amount of data. In postcontrast T_1 maps, focal fibrosis could be confirmed with late contrast-enhancement images.

Conclusion: The proposed approach provides high-resolution T_1 maps within 8 s. Data acquisition efficiency for T_1 mapping was improved by a factor of 5 by integration of cardiac motion correction, resulting in precise T_1 maps.

KEYWORDS

cine imaging, cardiovascular MR, motion correction, myocardial tissue characterization, T_1 mapping

This is an open access article under the terms of the Creative Commons Attribution License, which permits use, distribution and reproduction in any medium, provided the original work is properly cited.

© 2019 The Authors. *Magnetic Resonance in Medicine* published by Wiley Periodicals, Inc. on behalf of International Society for Magnetic Resonance in Medicine

1 | INTRODUCTION

Cardiovascular MR is a widely used imaging modality for the diagnosis of cardiac diseases. The quantification of T_1 relaxation is an important intrinsic marker to detect ischemic and nonischemic cardiomyopathies.¹⁻³

Postcontrast and native T_1 mapping are relevant for the characterization of pathological changes of myocardial tissue. Native myocardial T_1 has the potential to detect diffuse cardiomyopathies without the need of contrast media administration.^{4,5} Furthermore, the combination of native and post-contrast T_1 maps allows for calculation of the extracellular volume fraction, permitting quantification of diffuse fibrosis.⁶

Whereas respiratory motion may be largely suppressed by holding the breath during a 2D MR scan, cardiac motion is always present during data acquisition. Common myocardial T_1 mapping techniques therefore utilize electrocardiogram (ECG) triggering in which qualitative images with different TIs (TI images) are only acquired at 1 specific cardiac motion state, such as mid-diastole, after an inversion or saturation recovery preparation. However, such ECG-triggered acquisitions limit the amount of data used for image reconstruction to 10% to 20% per cardiac cycle, leading to low scan efficiencies.⁷⁻⁹ This is especially challenging for T_1 mapping because multiple TI images need to be obtained for the calculation of 1 quantitative T_1 map. In order to ensure clinically feasible breath-hold times, cardiac T_1 mapping is commonly limited in terms of spatial resolution. In addition, ECG triggering requires reproducible detection of each cardiac cycle during data acquisition. Heart rate variations or arrhythmia can lead to TI images, which are obtained in different cardiac phases, and the mismatch between these images could lead to errors in voxel-based T_1 mapping.^{9,10}

Continuous data acquisition with retrospective cardiac motion correction has been proposed for 3D anatomical cardiovascular MR in order to improve scan efficiencies and make data acquisition not reliant on accurate ECG-triggering.^{11,12} For quantitative cardiovascular MR, thus far only

respiratory motion correction has been explored to improve parameter map quality.¹³⁻¹⁸ These techniques correct for small residual respiratory motion in breath-held and free-breathing acquisitions. Cardiac motion leads to a more complex deformation of the heart than respiratory motion. Therefore, accurate cardiac motion estimation requires high-quality cardiac motion-resolved images with constant and high contrast between myocardium and blood.

In this study, we present a cardiac motion-corrected T_1 mapping approach with an increased T_1 mapping efficiency for high-resolution T_1 mapping. This is done by continuous acquisition, allowing reconstruction of cine MRI and TI images from the same data. Nonrigid cardiac motion estimation was integrated to correct for motion before carrying out voxel-based T_1 mapping. The approach was evaluated in 10 healthy volunteers for native T_1 mapping. Furthermore, clinical feasibility was tested in 5 patients with suspected myocardial fibrosis after contrast agent administration by comparing postcontrast T_1 maps to late gadolinium enhancement (LGE) images, which is the gold standard modality for detection of focal fibrosis.

2 | METHODS

The proposed approach can be separated into 3 steps: First, cine images are reconstructed from the acquired 2D golden angle radial data. In a second step, these images are registered to obtain nonrigid motion fields describing the cardiac movement of each voxel during the cardiac cycle. Lastly, cardiac phase-resolved images are reconstructed for different TIs from the same data. Each cardiac phase is transformed to a reference phase using the motion fields obtained in step 2. Systolic cardiac phases were excluded due to through-plane motion allowing for 80% of the total scan time to be used for T_1 mapping. A voxel-wise 3-parameter T_1 fit is applied to obtain the final quantitative cardiac motion-corrected T_1 maps.

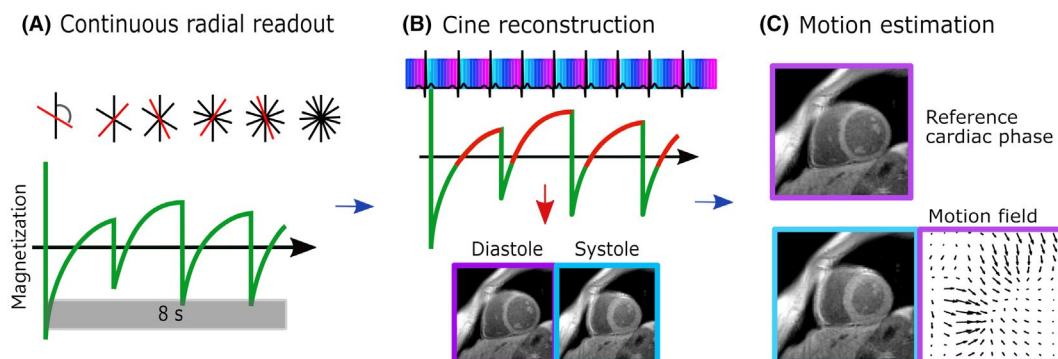


FIGURE 1 Data acquisition and cardiac motion estimation. (A) Data is continuously acquired with golden angle radial readout. Multiple inversion RF-pulses were applied. (B) Cine images with 15 cardiac phases were reconstructed prior to T_1 mapping. Only part of the data (red) is used for reconstruction to guarantee a constant contrast over all cardiac phases. Negative signal associated with healthy myocardium is rejected (dashed line). (C) For each cardiac phase, a cardiac motion field is obtained

2.1 | Data acquisition

2D slices were acquired continuously by a low flip angle spoiled-gradient echo sequence with golden angle radial sampling, an angular increment of 111.25° ,¹⁹ and employing adiabatic inversion recovery preparation at constant time intervals (Figure 1). Data was acquired within a breath-hold on 3 Tesla (Verio, Siemens Healthineers, Erlangen, Germany)—flip angle: 5° , TE/TR: 2.03/4.93 ms, FOV: $320 \times 320 \text{ mm}^2$, 2-fold oversampling in radial direction, resolution: $1.3 \times 1.3 \times 8.0 \text{ mm}^3$. Nonselective inversion RF-pulses were applied every 2276 ms. The ECG was recorded for retrospective cardiac gating and data selection. Total acquisition time per slice was 8 s.

2.2 | Cine reconstruction

Data was retrospectively binned into 15 cardiac motion states using the ECG signal providing cardiac motion-resolved images (I_{Cine}^{1-15}) (Figure 1B). The contrast over the entire scan is not constant due to the application of multiple inversion pulses. Nevertheless, each image I_{Cine} is reconstructed from data at various time points after the inversion pulses. This leads to an average contrast for I_{Cine}^{1-15} , which is constant over all reconstructed cardiac motion states. In order to enhance the contrast between blood and myocardium, data was only used for cine reconstruction if the signal intensity of myocardium was positive. Data acquired immediately after all inversions was therefore excluded for reconstruction depending on the T_1 times associated with healthy myocardium. In noncontrast-enhanced imaging, data obtained 1175 to 2276 ms after the first inversion and 400 to 2276 ms after all other inversions were included (Figure 1B). Thus, only the positive signal of myocardium is used. Blood has a longer native T_1 time, so the signal from blood is lower and partly negative, resulting in dark blood images. The acceleration factor of native cine images was 5.0. In contrast-enhanced imaging, only 200 ms after each inversion were excluded due to shorter T_1 times. Here, myocardial T_1 is longer than T_1 of blood, resulting in a higher blood signal in the corresponding cine images and thus bright blood images. I_{Cine}^{1-15} were reconstructed iteratively using spatial and temporal total variation regularization (10 iterations, $\lambda_{\text{spatial}}: 10^{-6}$, $\lambda_{\text{temporal}}: 5 \times 10^{-6}$).²⁰ All image reconstruction was performed offline in MATLAB 2016b (MathWorks, Natick, MA).

2.3 | Motion estimation

Nonrigid cardiac motion estimation was performed on the cine images. For the reference cardiac phase, a mid-diastolic phase was used. For image registration, a free-form deformation algorithm²¹ was used, which was composed of a cubic B-spline interpolation scheme as deformation model, normalized mutual information as similarity metric, and bending energy as penalty term (NiftyReg).²² A rectangular region of

interest covering both ventricles was selected in a first step to accelerate motion estimation. No segmentation of myocardial contours was needed. Motion estimation yielded 1 cardiac motion field per cardiac motion state (MF^{1-15}) describing the transformation from each cardiac phase to the reference motion state (Figure 1C). In order to test motion estimation, these motion fields are applied to each cardiac phase, that is, $\text{MF}^{1-15} \circ I_{\text{Cine}}^{1-15}$, transforming all cardiac phases to the same motion state and thus providing a motion-corrected image sequence.

2.4 | Signal model of longitudinal magnetization

The longitudinal magnetization M during continuous spoiled gradient echo acquisition after an inversion pulse can be described as Look-Locker concept.²³

In our model, the inversion recovery Look-Locker concept was extended to multiple inversions with a constant time between the inversion (T_{ic}) to characterize the longitudinal magnetization of the entire data acquisition without magnetization recovery periods²⁴:

$$M(t) = M_0^{eff} - \left(M_j^+ + M_0^{eff} \right) \exp \left(- \frac{t - (j-1)T_{ic}}{T_1^{eff}} \right), \quad (1)$$

where j is the number of the applied inversions at a specific time point, and M^+ is the magnetization right before the next inversion. M_0 is proportional to the spin density, and T_1^{eff} describes the effective relaxation time when a low flip angle α is applied²³:

$$T_1^{eff} = \left[1/T_1 - (1/TR \ln(\cos(\alpha))) \right]^{-1}. \quad (2)$$

In this model, M_0^{eff} is the steady state magnetization

$$M_0^{eff} = M_0 T_1^{eff} T_1^{-1}. \quad (3)$$

For robustness of the fitting, the inversion efficiency is assumed to be 1.

2.5 | Motion-corrected T_1 mapping

Cardiac motion-corrected T_1 mapping (T_1^{moco}) contains the following steps (Figure 2):

1. *Gating*: Data was retrospectively gated, yielding exactly the same 15 cardiac motion states as in cine reconstruction. In contrast to the cine reconstruction before, 15 phases for each cardiac cycle are obtained (i.e., real-time sequence) rather than retrospectively combining data from multiple cardiac cycles.
2. *Data selection*: Based on the reconstructed cine images of the same acquisition, 3 systolic motion states were

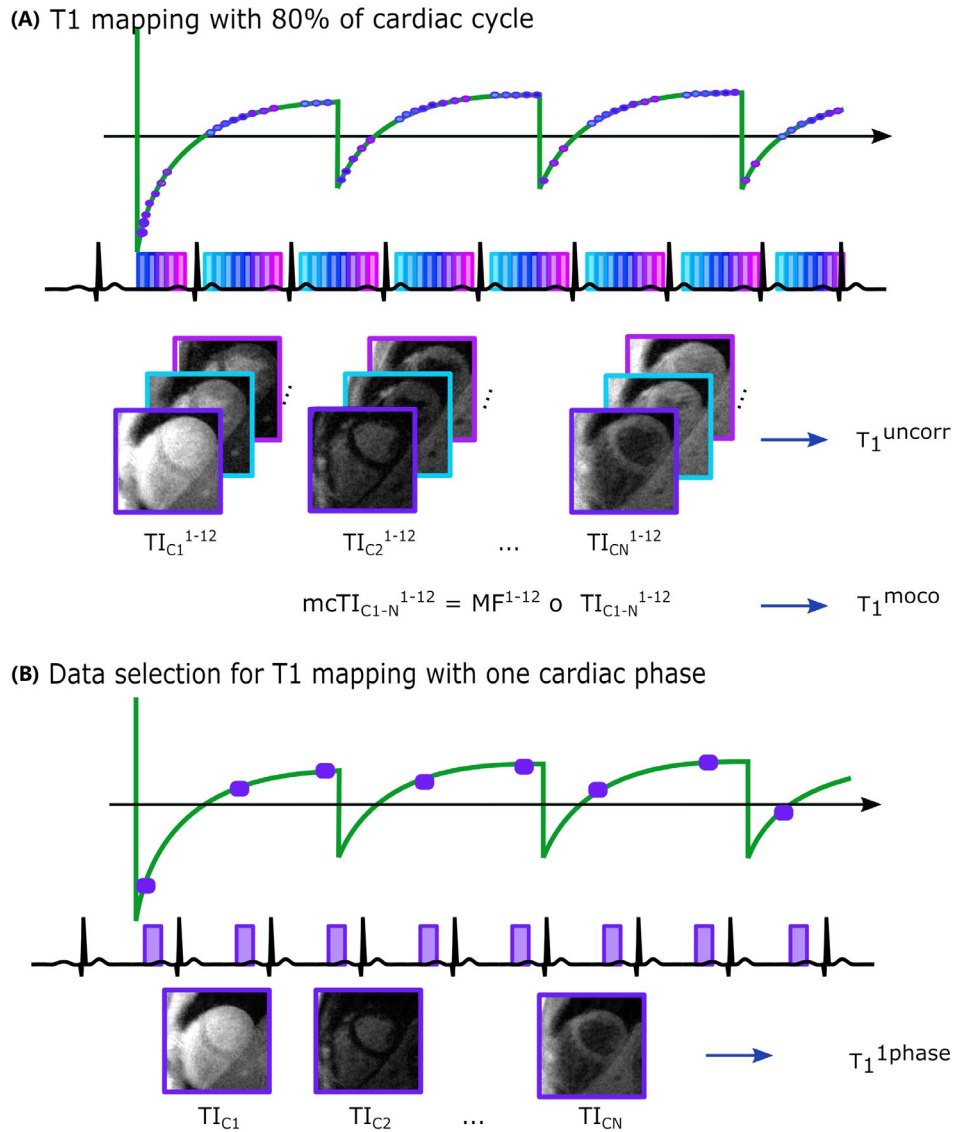


FIGURE 2 T₁ mapping. (A) T₁ mapping using 80% of the cardiac cycle. The cardiac cycle is split into the same cardiac phases as for cine reconstruction, leading to 15 qualitative images per cardiac cycle and 3 midsystolic images were excluded. Cardiac motion is corrected in TI images and T₁ is fitted, leading to T₁^{moco}. Furthermore, T₁ is also fitted on motion-uncorrected TI images (T₁^{uncorr}). (B) For comparison purpose, T₁ mapping is performed using reconstructed TI images of only 1 cardiac phase of the same data acquired as in (A) (T₁^{1phase}). The window length was 168 ms per cardiac cycle, comparable to a standard T₁ mapping approach

excluded in each cardiac cycle to minimize through-plane motion artifacts in the T₁ maps, which cannot be corrected for in a 2D acquisition.

3. *Image reconstruction*: In each cardiac cycle (C1 to C_n), 12 highly undersampled TI images (TI¹⁻¹²) were reconstructed of the same cardiac motion states as selected for cine reconstruction (TI_{C1-Cn}¹⁻¹²). TI images were reconstructed using non-Cartesian iterative SENSE²⁵ without temporal or spatial filtering of the data. The total data window for T₁ mapping was 80% per cardiac cycle, divided into 12 TI images.
4. *Motion correction*: Prior to T₁ mapping, corresponding inverse deformation fields iMF^{1-12} were applied to all TI images TI_{C1-Cn}¹⁻¹². Thus, 12 motion-corrected TI images were obtained for each cardiac cycle: $mcTI_{C1-Cn}^{1-12} = MF^{1-12} \circ TI_{C1-Cn}^{1-12}$.

5. *T₁ estimation*: T₁, M₀, and the flip angle were estimated by a voxel-wise 3-parameter fit of the magnitude $mcTI_{C1-Cn}^{1-12}$ images to the signal model.¹

Two additional T₁ maps were calculated based on the same raw data. To verify the influence of motion correction on T₁ estimation, the same TI images were selected as above; however, no motion correction step was performed prior to T₁ mapping, yielding T₁^{uncorr} maps. Besides this, the influence of the increased amount of k-space lines compared to standard cardiac triggered T₁ mapping approaches was evaluated. For this, data during mid-diastole was selected within a single window per cardiac cycle with a duration of 168 ms.²⁴ Here, the quality of each TI image is better due to the larger window length and thus

more available k-space data per T₁ image, but total amount of data used for T₁ mapping is lower. These T₁ maps are called T₁^{1phase} maps throughout the study.

2.6 | Phantom experiment

To evaluate the proposed approach, imaging was performed with the above-described scan parameter in the TIMES phantom, with 9 different T₁ times investigated for cardiac applications.²⁶ Furthermore, an inversion-recovery spin echo method was applied for the reference with 7 TIs between 25 and 4800 ms (TE/TR: 12/8000 ms, FOV: 130 × 160 mm², and spatial resolution: 1.3 × 1.3 × 8 mm³). T₁ times were estimated based on a 2-parameter fit for T₁ and M₀. Additionally, a 5(3)3 modified Look-Locker inversion recovery (MOLLI) was applied with the following scan parameter—FOV: 360 × 306 mm², TE/TR: 1.12/2.70 ms, flip angle: 35°, and spatial resolution: 2.1 × 1.4 × 8.0 mm³.

2.7 | Native T₁ mapping

The approach was applied without contrast administration in 10 healthy subjects (6 males/4 females, aged 31.3 ± 8.4 years) in a midventricular short axis (SAX) orientation. A stack of 9 SAX images was obtained in 1 healthy volunteer (male, 34 years) with the approach and 5(3)3 MOLLI. In accordance with the institutions' ethical committees, all participants gave written informed consent before examination. In order to study potential effects on different scan orientation, additional images were obtained in 4-chamber view in 2 of the subjects. T₁^{moco}, T₁^{1phase}, and T₁^{uncorr} maps were calculated for each acquisition.

2.8 | Postcontrast T₁ mapping in patients with suspected focal fibrosis

To test feasibility of the approach for the detection of fibrosis, 5 subjects with suspected focal fibrosis were scanned (3 female/2 male, age: 60.6 ± 8.4 years, height: 168.8 ± 9.7 cm, weight: 76.0 ± 12.1, body mass index: 26.9 ± 5.2). The patients were included as part of the Berlin Longterm Observation of Vascular Events study. This study was approved by the local ethic committee (EA1/066/17), and all subjects gave written informed consent. To detect focal fibrosis, a stack of SAX LGE phase-sensitive inversion recovery images with gradient echo readout was acquired 15 minutes after contrast administration (0.15 mmol/[kg body weight] gadoteridol) with the following scan parameter: flip angle: 20°, TE/TR: 1.56/4.10 ms, acquisition time: 10 heartbeats, spatial resolution: 2.1 × 1.4 × 7.0 mm³, FOV: 350 × 263 mm², which was adapted to the patient. For postcontrast T₁ mapping, 1 2D slice was acquired such

that fibrotic tissue was best visible, and T₁^{moco}, T₁^{1phase}, and T₁^{uncorr} maps were calculated.

2.9 | Analysis

In the phantom, T₁ times were averaged over each tube. Pearson's linear correlation was tested, and differences in T₁ time between the reference and the proposed approach as well as the reference and MOLLI were calculated and averaged over all tubes.

In vivo analysis was performed in midventricular SAX images. Six midventricular myocardial segments of the left ventricle, adapted from the American Heart Association consensus statement, and the left ventricular blood pool were segmented.²⁷ Segmentation and evaluation were performed using in-house software in MATLAB 2016b (MathWorks).

Motion fields³³ were applied to the cine images (MF¹⁻¹⁵ ∘ I_{Cine}¹⁻¹⁵) in order to visually assess motion correction. To investigate the amplitudes of estimated motion, the deformation fields of each cardiac motion state were quantified. For quantification, the norm of the 2D deformation vectors in each voxel were averaged over all 6 segments for each cardiac phase. The maximum deformation was determined in each subject and averaged over all volunteers. After exclusion of 3 systolic phases, the remaining maximum deformation was averaged over all volunteers. Additionally, the deformation was additionally obtained over the highest 10% of each segment and cardiac phase; subsequently, the highest deformation was averaged over all volunteers.

To test reproducibility of the motion estimation, an additional test was performed on the motion fields. Estimated inverse motion fields of the 12 included cardiac phases were applied to the reference cine images (iMF¹⁻¹² ∘ I_{Cine}^{ref}). In a second step, these obtained cine images were again registered to I_{Cine}^{ref}, obtaining new cardiac motion fields. This was done for all 10 healthy subjects. Differences between both motion fields were calculated for each cardiac phase and each segment.

Native and postcontrast T₁ times were assessed in all myocardial and blood segments. Normal distribution of T₁ times was tested by a Shapiro-Wilk test. To verify overall effects of the T₁ mapping method on T₁ times, T₁ times of T₁^{moco}, T₁^{1phase}, and T₁^{uncorr} maps were averaged over the 6 segments and compared using a Friedman test with Dunn's multiple comparison correction.

In this study, the SD of T₁ times across a segment (spatial variability) was used to quantify the precision of the measurement in healthy subjects because in healthy volunteers the T₁ times of the myocardium can be assumed to be constant.

The SD of native T₁ was determined in each segment. Normal distribution of SDs was tested by a Shapiro-Wilk test. Overall differences in SD between the 3 methods were assessed by a comparison of the SD over the whole

myocardium between T_1^{moco} , T_1^{1phase} , and T_1^{uncorr} maps by analysis of variance with Tukey's multiple comparison correction across the 10 healthy volunteers. For comparison to MOLLI, T1 times were assessed segment-wise in basal, midventricular, and apical slices and averaged. Spatial variation was averaged over all segments for analysis of precision.

In postcontrast T_1^{moco} maps with visible focal fibrosis, T_1 times of fibrotic segments were assessed, and T_1^{moco} values of the fibrotic segment were compared against T_1 values of all healthy segments using a Kruskal-Wallis test. The statistical analysis was performed in GraphPad Prism 6, and $P < 0.05$ was considered to be significant.

3 | RESULTS

3.1 | Phantom experiment

Cardiac motion-compensated T_1 mapping and MOLLI showed good correlation with the reference scan ($R^2 > 0.99$). Relative differences between the reference and both techniques averaged over all tubes were $0.28\% \pm 3.70\%$ (-5.42% to 3.88%) using our approach and $1.43\% \pm 1.99\%$ (-1.42% to 4.61%) using 5(3)3 MOLLI. A comparison between the

reference and our approach can be found in Supporting Information Figure S1.

3.2 | Cine reconstruction

Cine images had a consistent contrast over all cardiac phases, which can be observed in the temporal slice profiles of Figures 3 and 4. Noncontrast-enhanced images resulted in a dark-blood contrast (Figure 3), and postcontrast cine images showed a bright-blood contrast (Figure 4) due to longer myocardial postcontrast T_1 times compared to blood. The temporal resolution of each cardiac phase was between 55 and 87 ms, depending on the heart rate (46 to 73 beats per minute [bpm]), and only few streaking artefacts were present in cine images.

3.3 | Motion estimation

Motion estimation succeeded in all volunteers, with only small residual motion in cardiac motion-corrected cine images ($MF^{1-15} \circ I_{\text{Cine}}^{1-15}$). The effect of motion correction can also be seen in the temporal slice profiles of the cine images in Figures 3 and 4. Animated cine images with and without

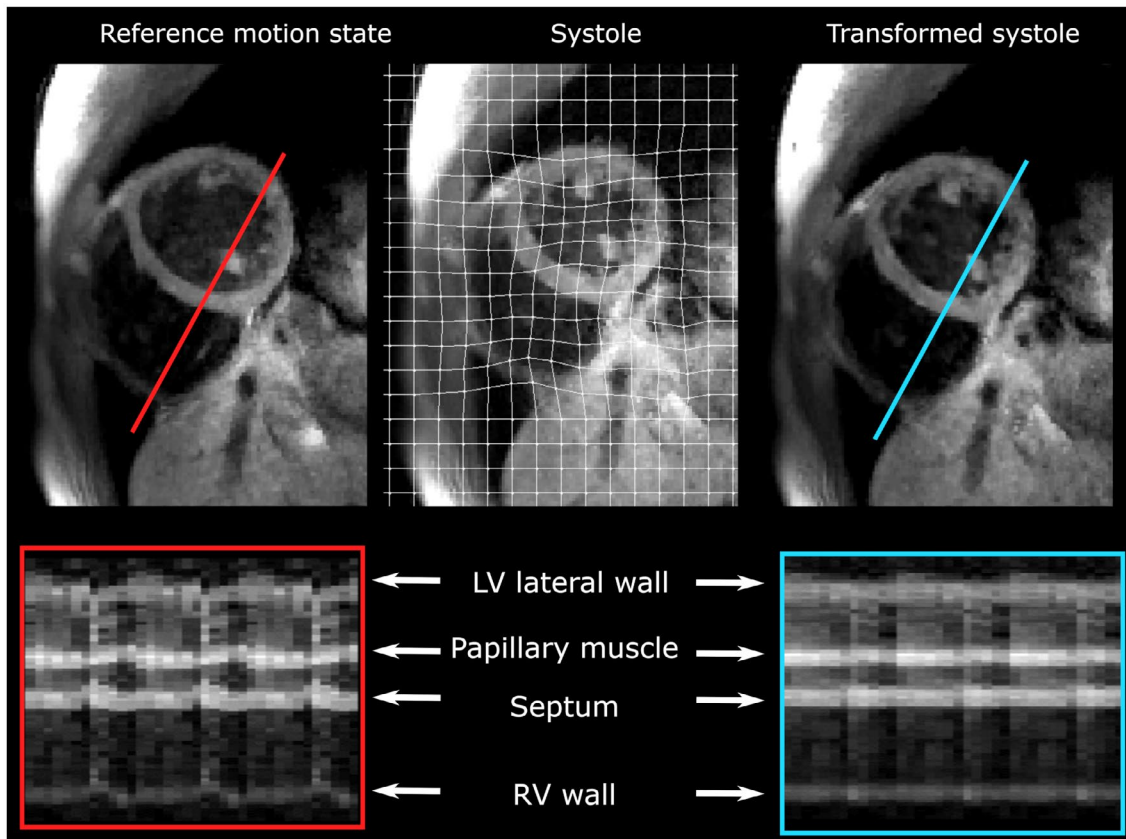


FIGURE 3 Cine images and motion correction without contrast administration. The deformation of the heart is estimated for each cardiac phase (middle), and motion is corrected (right) to match the reference mid-diastolic phase (left). The temporal slice profiles of cine images excluding 3 systolic phases are shown in the lower row (red line). Animated cine images with and without motion correction can be found in the Supporting Information Video S1

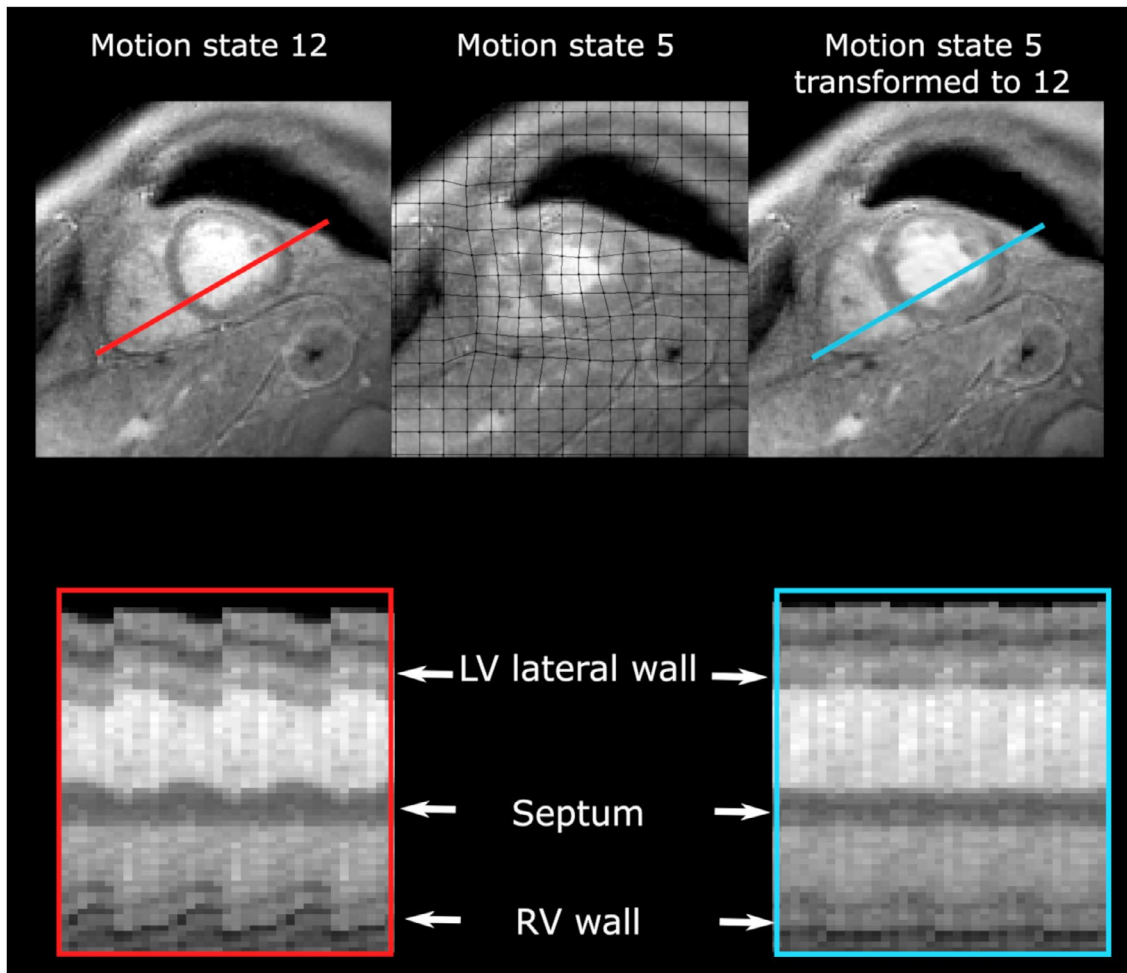


FIGURE 4 Cine images and motion correction after contrast administration. The deformation of the heart is estimated for each cardiac phase (middle), and motion is corrected (right) to match the reference mid-diastolic phase (left). The temporal slice profiles of cine images excluding 3 systolic phases are shown in the lower row (red line). Animated cine images with and without motion correction can be found in the Supporting Information Video S2

motion correction, in which 3 systolic motion states were already excluded, can be found in Supporting Information Video S1 (precontrast) and Supporting Information Video S2 (postcontrast), and motion fields of all cardiac phases are shown in Supporting Information Video S3. The highest deformation over the whole myocardium and all healthy subjects was 4.51 ± 0.98 mm in systole. Excluding 3 systolic motion states, the remaining highest deformation was still 3.30 ± 0.88 mm. This averaged deformation underestimates the maximum deformation of the myocardium due to large variations over the myocardium. The highest deformation in healthy subjects was 7.54 ± 1.89 mm. The estimated motion per cardiac phase depended strongly on the heart rate, with an averaged motion of more than a voxel length of 1.3 mm in only 5 of 15 cardiac phases for a very low heart rate (46 bpm) and 9 cardiac phases for a higher heart rate (66 bpm) (Figure 5A).

The repeatability experiment showed small differences between motion estimations. Differences between both motion estimations were $0.25 \text{ mm} \pm 0.17 \text{ mm}$ [0.04 to 1.32 mm],

averaged over all 15 cardiac phases, segments, and volunteers. Only in 1 systolic cardiac phase of 1 healthy volunteer was the error in the range of the voxel size (1.32 mm).

3.4 | Native T_1 mapping

In SAX orientation as well as 4 chamber view, motion-corrected T_1 maps had less blurring and partial volume effects compared to uncorrected T_1 maps (Figures 6 and 7). The myocardium and papillary muscles can be well distinguished in the T_1^{moco} maps. T_1 maps obtained with 80% of the cardiac cycle (T_1^{uncorr} and T_1^{moco}) showed lower SD than T_1^{phase} maps. The total amount of data used for T_1^{moco} and T_1^{uncorr} mapping was on average 5.2 (4.3 to 6.8) times higher compared to T_1^{phase} mapping, with undersampling factor of 22.2 to 34.3 for each TI image. Maps of all fitted parameters can be found in Supporting Information Figure S2.

In Figure 5, the influence of cardiac motion on T_1^{uncorr} maps is shown for different heart rates. The main

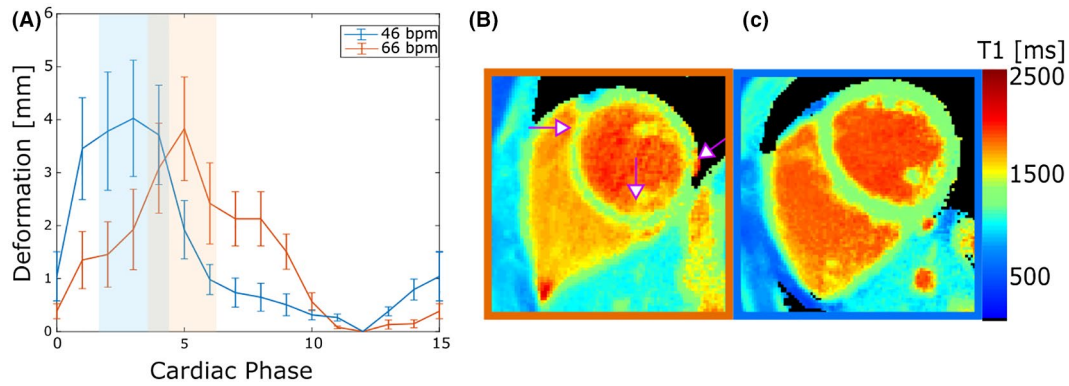


FIGURE 5 Impact of motion on uncorrected T_1 map at different heart rates. (A) Estimated cardiac motion averaged over all 6 segments per cardiac phase (mean \pm SD). For normal heart rates, even after excluding systolic phases, motion amplitudes are larger than the spatial resolution of 1.3 mm for most cardiac phases (orange). In the corresponding T_1^{uncorr} map (B), motion led to wrong T_1 estimation. For low heart rates, only a few cardiac phases show motion amplitudes larger than the voxel size (blue), and no motion artifacts are visible in the corresponding T_1^{uncorr} map after exclusion of 3 systolic phases (C)

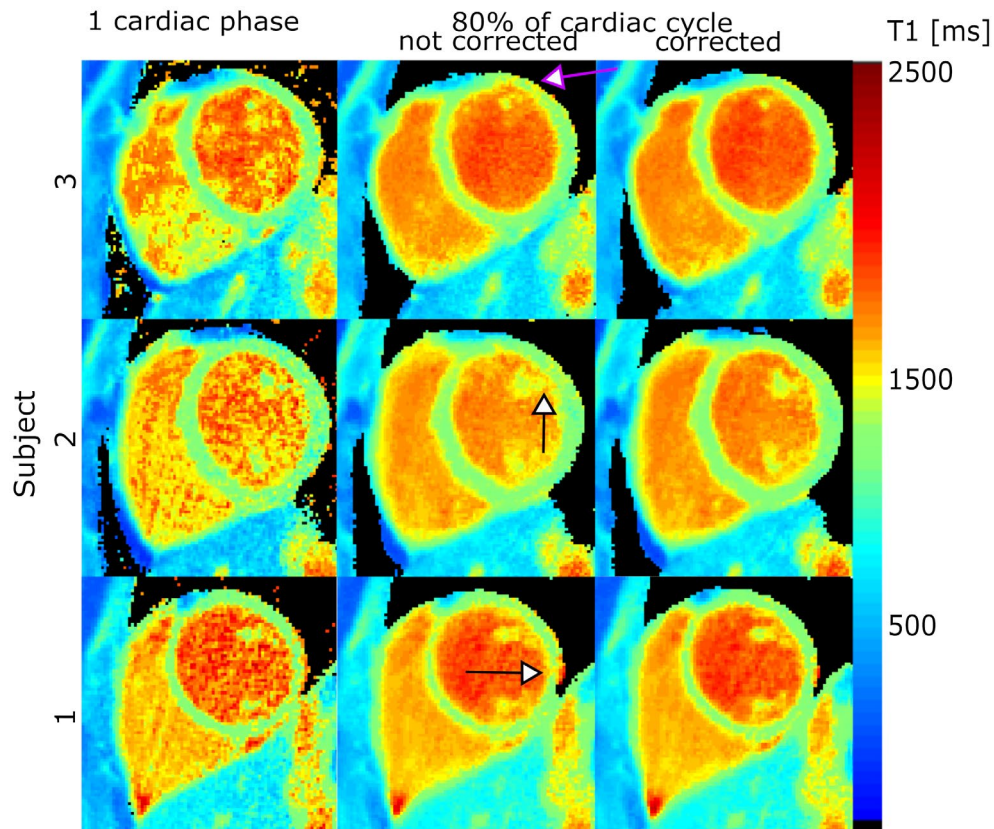


FIGURE 6 Native T_1 maps of 3 healthy subjects. T_1 maps estimated using 1 cardiac phase (T_1^{1phase} , left) showed higher SD compared to T_1 maps calculated from images covering 80% of each cardiac cycle. In motion-uncorrected T_1 maps (T_1^{uncorr} , middle), motion led to blurring and partial volume effects (arrows), which is not present in motion-corrected T_1 maps (T_1^{moco} , right)

difference between the high and low heart rate was that, after leaving out 3 systolic phases (marked as blue area), only 2 cardiac phases show a deformation larger than a voxel length of 1.3 mm for a low heart rate (46 bpm). For the higher heart rate (66 bpm), 6 remaining cardiac phases show a deformation larger than 1.3 mm. Therefore, the impact of cardiac motion on the final image quality is

higher for the high heart-rate case than for the low-heart rate case (Figure 5B,C). However, for heart rates in the normal range or higher (here shown for 66 bpm), cardiac motion resulted in inaccurate estimation of myocardial T_1^{uncorr} , which can be observed by regional prolonged T_1 times due to a mismatch of motion state in uncorrected T1 images (Figure 5B).

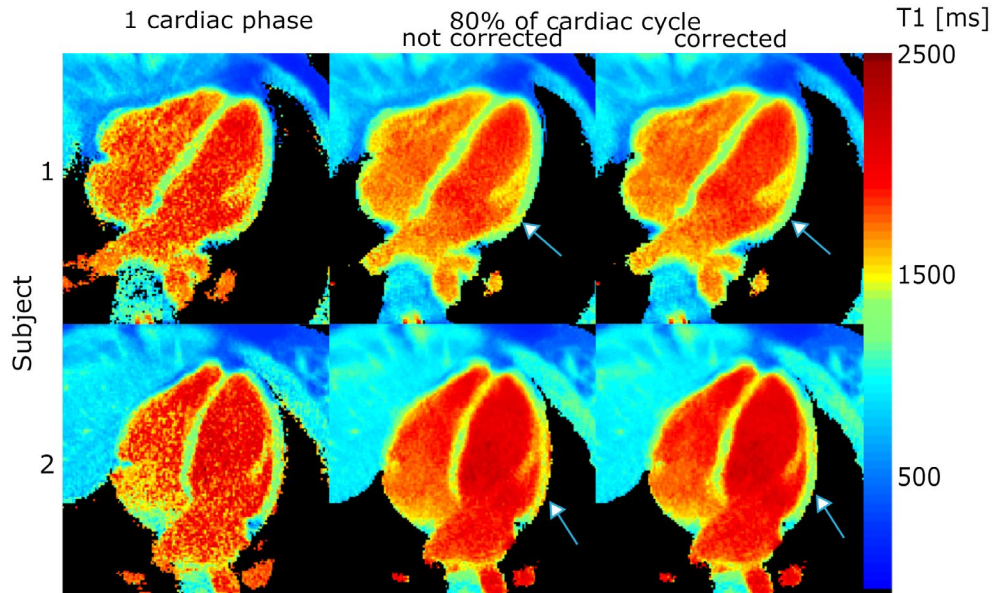


FIGURE 7 Native T_1 maps in 4 chamber view. Cardiac motion-corrected T_1 mapping is not restricted to short-axis orientation. Motion-corrected T_1 maps showed better T_1 mapping quality than uncorrected T_1 maps, especially in the lateral wall of the left ventricle (arrows). T_1 maps using 80% of the cardiac cycle showed visually a lower spatial variation of T_1 compared to T_1 mapping with only 1 cardiac phase

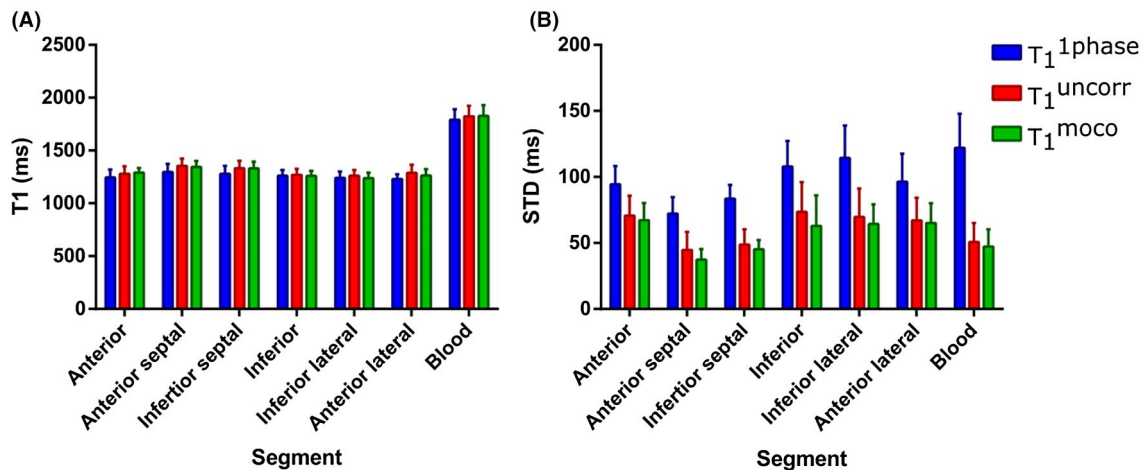


FIGURE 8 T_1 times and spatial variation of T_1 (SD). (A) T_1 times across healthy subjects in 6 myocardial segments and in the left ventricular blood pool of each segment (mean \pm SD). Motion-compensated T_1 and T_1 obtained with only 1 cardiac phase did not differ significantly. (B) The T_1 SD of the motion-corrected T_1 across healthy volunteers was significantly lower in all segments compared to T_1 maps obtained with only 1 cardiac phase and motion uncorrected T_1 ($P = 0.036$ and $P < 0.0001$, respectively)

T_1 times and SDs of all myocardial segments and blood are shown in Figure 8. $T_1^{1\text{phase}}$, T_1^{uncorr} , and T_1^{moco} times of the whole myocardium across all healthy volunteers were 1259 ± 55 ms, 1298 ± 60 ms, and 1288 ± 49 ms, respectively (Figure 8A). T_1^{uncorr} times were significant longer than $T_1^{1\text{phase}}$ times ($P = 0.008$), whereas no significant differences were found between T_1^{moco} and $T_1^{1\text{phase}}$ ($P = 0.281$), as well as between T_1^{moco} and T_1^{uncorr} ($P = 0.539$).

The SD of T_1 within the myocardium was highest in $T_1^{1\text{phase}}$ maps, with 94.8 ± 15.4 ms (Figure 8B). T_1^{uncorr} maps had a significant lower SD compared to $T_1^{1\text{phase}}$ maps (62.44 ± 10.2 ms,

$P < 0.0001$). By the integration of motion correction, the SD was further reduced (57.0 ± 12.5 ms, $P = 0.0356$). T_1^{moco} maps had a 40% lower SD in the myocardium compared to $T_1^{1\text{phase}}$ maps across the healthy subjects ($P < 0.0001$). In blood, the SD was 53% lower in T_1^{moco} compared to $T_1^{1\text{phase}}$ ($P < 0.0001$). No cardiac motion artefacts were observed in $T_1^{1\text{phase}}$ maps. T_1^{moco} maps of the different slice positions of the stack of SAX slices were comparable to MOLLI (Figure 9). Basal, midventricular, apical, and blood T_1 times were 1217 ± 17 ms, 1196 ± 37 ms, 1224 ± 43 ms, and 1898 ms in MOLLI, respectively. In T_1^{moco} maps, T_1 times were 1272 ± 40 ms, 1267 ± 35 ms,

1312 ± 20 ms, and 1776 ms, respectively. Spatial variation was 46.5 ± 17.21 ms for MOLLI and 55.68 ± 17.71 ms for our approach.

3.5 | Postcontrast T_1 mapping

In postcontrast T_1 mapping, slices were oriented in basal (subject C) and midventricular short-axis orientation (subject A and B). In the LGE images, focal fibrosis was visible in 2 patients. In subject B, focal fibrosis was depicted in a lateral segment, and even small focal fibrotic spots were detected in the anterior segment of subject C (Figure 10). In the subjects without focal fibrosis, T_1 times were homogenous over the myocardium (subject A).

Postcontrast T_1 mapping was successful with the same acquisition as for native T_1 mapping. In postcontrast T_1^{uncorr} maps, different motion states of the TI images led to blurring of the myocardial border. In T_1^{moco} maps, the border between blood and myocardium was better defined than in T_1^{uncorr} maps. In postcontrast T_1^{moco} maps, focal fibrosis could be detected at the same location as in the LGE images. In these spots, T_1 times were shorter compared to surrounding healthy tissue. In the 2 subjects with focal fibrosis, the averaged T_1^{moco} of the fibrotic segment were -69.5 ± 11.9 ms and -51.8 ± 12.0 ms shorter compared to all healthy segments

in the same subject ($P < 0.002$ for all segments) (Figure 9). In T_1^{uncorr} maps, differences were -67.3 ± 14.2 ms and -28.6 ± 17.4 ms, and small fibrotic spots were poorly visible in these T_1 maps. In T_1^{1phase} maps, differences were 60.5 ± 19.3 ms and 46.4 ± 14.3 ms.

4 | DISCUSSION

In this study, a novel cardiac motion-corrected T_1 mapping approach was presented that provides high-resolution T_1 maps in a short 8 s breath-hold. Scan efficiency was increased by continuous data acquisition and correction for cardiac motion. Hereby, it was possible to use 80% of the total scan time for T_1 mapping instead of only about 20%. Thus, the amount of data used for T_1 mapping was increased by a factor of 5 compared to a cardiac-triggered T_1 mapping approach. Cardiac motion estimation was carried out from the same raw data used for T_1 mapping. An increase in precision compared to a cardiac triggered approach using only 1 specific motion state was demonstrated, and feasibility for postcontrast T_1 mapping in patients was shown.

The spatial variation of T_1 times (SD) in healthy myocardium is related to the precision of the measurement. By integration of motion correction, the precision of T_1 mapping was improved compared to T_1^{uncorr} mapping, which could be explained by less blurring in T_1^{moco} maps. Improved sharpness could be important for the detection of small epi- or endocardial fibrosis.

The individual TI images of T_1^{moco} and T_1^{uncorr} were reconstructed from data acquired in a 55 to 87 ms window compared to the 3 times longer window used for T_1^{1phase} mapping. Therefore, the TI images of T_1^{moco} and T_1^{uncorr} showed higher undersampling artifacts. Nevertheless, for the voxel-wise T_1 fit, 12 TI images per cardiac cycle were used for T_1^{moco} and T_1^{uncorr} rather than 1 for T_1^{1phase} . This led on average to 5.2 (4.3 to 6.8) times more data being utilized for the T_1^{moco} fitting. For the proposed golden angle radial acquisition, the undersampling artifacts between different TI images were incoherent along the recovery curve; thus, a robust T_1 fit was achieved,²⁸ leading to more reproducible T_1 times and an increase in precision by 34% compared to the standard T_1^{1phase} mapping.

In vivo T_1 times obtained with T_1^{uncorr} , T_1^{moco} , and T_1^{1phase} mapping varied slightly, but all were within the range of previously published native T_1 times at 3 Tesla. Compared to those studies, T_1 times were longer than MOLLI, also observed in our study, and longer than shortened MOLLI plus multitasking,²⁹⁻³¹ but shorter than SASHA and SAPPHERE.³² A study evaluating the precision of different T_1 mapping approaches showed a comparable precision in MOLLI and SAPPHERE (54.0 and 58.6 ms, respectively) and a lower precision of SASHA compared to our approach (68.2 vs. 57.0 ms).³² However, comparison to other studies is difficult due to

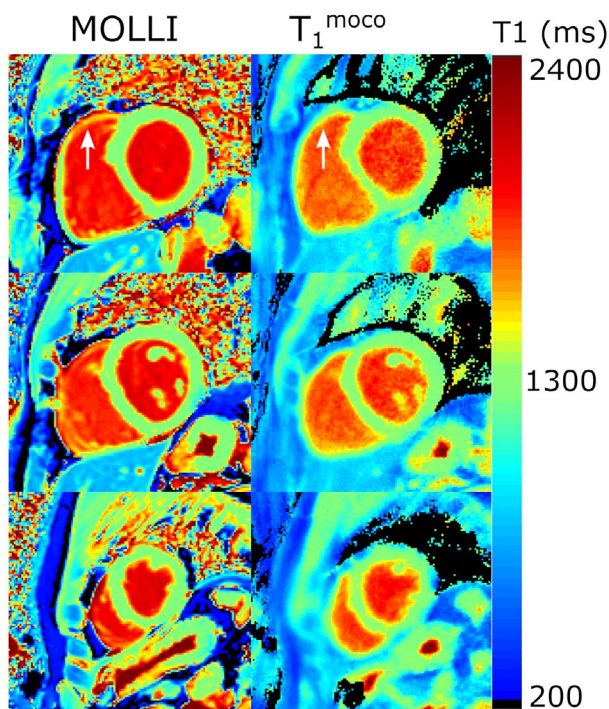


FIGURE 9 Comparison of MOLLI and motion-corrected T_1 maps in a basal (upper row), midventricular (middle), and apical (lower row) SAX slices. T_1^{moco} mapping was possible for all slices and visually comparable to MOLLI. The right ventricle was better defined in T_1^{moco} maps compared to MOLLI for all slices (arrows). MOLLI, modified Look-Locker inversion recovery; SAX, short axis

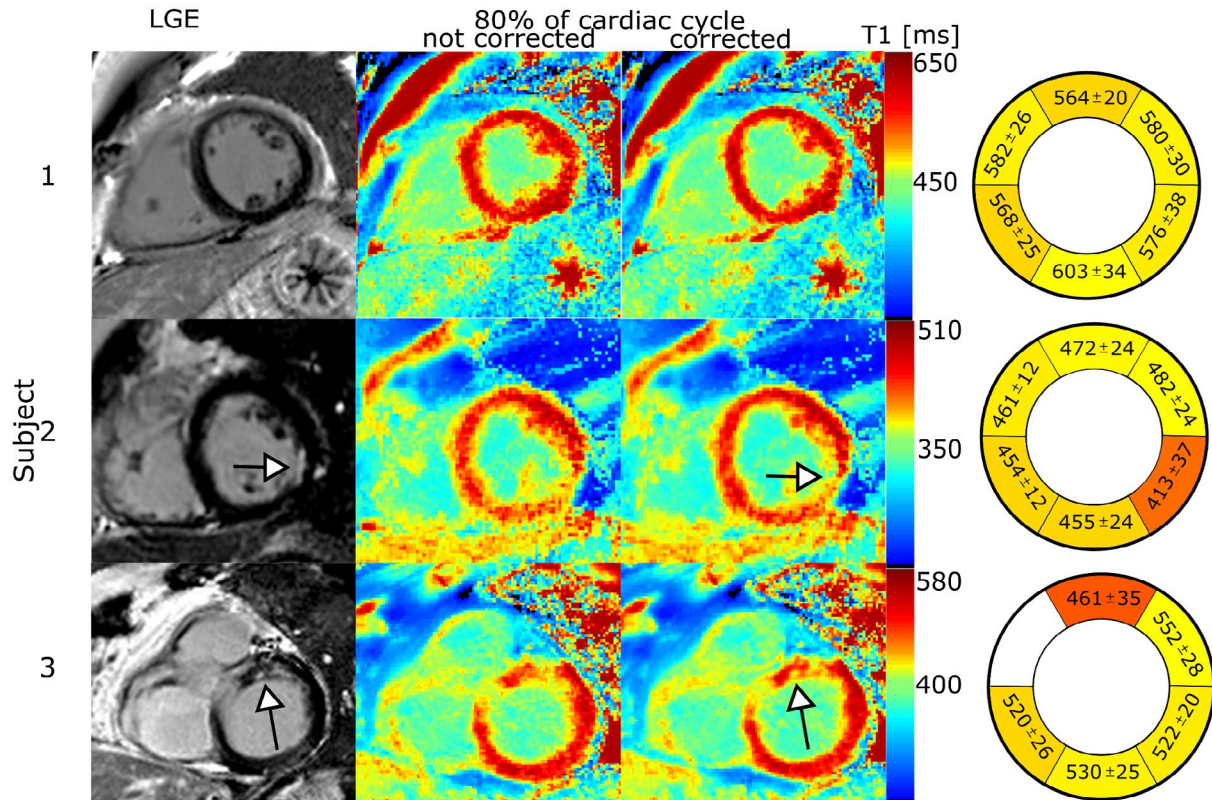


FIGURE 10 LGE images, postcontrast T_1 maps, and bull's-eye plots. The myocardium was more precisely defined in T_1^{moco} maps (right) compared to uncorrected T_1 maps (T_1^{uncorr} , middle). In subject A, no focal fibrosis is present and T_1 times are homogenous over the myocardium. In subject B and C, focal fibrosis can be visually depicted in T_1^{moco} maps and confirmed by LGE images obtained at same slice position (arrows). In subject B and C, T_1 times in the fibrotic segment were shorter compared to all healthy segments of the same subject (subject B: -69.5 ± 11.9 ms and subject C: -51.8 ± 12.0 ms, $P < 0.002$). In subject C, the segment intersecting the left ventricular outflow tract was excluded in the analysis

differences in acquisition and reconstruction settings as well as postprocessing procedures such as spatial filtering and the number of fit parameters, strongly affecting the precision.⁹

Radial sampling is very robust in the presence of physiological motion. Therefore, good quality T_1 maps can also be obtained for T_1^{uncorr} mapping, especially for subjects with low heart rates. Figure 5 shows that for a volunteer with a heart rate of 46 bpm, removing 20% of the data in systole leads to TI images in which the residual cardiac motion is below the spatial resolution of the images in more than 80% of the remaining cardiac phases. Therefore, the T_1 fit is mainly determined by these 80%, leading to a high-quality T_1 map. For a volunteer with a heart rate in the normal range (66 bpm), removing 20% of data still leaves 60% of data with residual cardiac motion larger than the voxel size. In that case, T_1 fitting is impaired by cardiac motion, and the obtained T_1 map shows severe motion artifacts due to motion state mismatches in TI images.

The separation of data into different cardiac phases both for the cine reconstruction and T_1 mapping was carried out retrospectively. The selection of the systolic phases to be removed prior to motion-corrected T_1 fitting was done based

on the reconstructed cine images rather than using a predefined delay time. Having the flexibility to retrospectively optimize the data selection can be especially important for arrhythmic patients in order to minimize errors due to ECG mistrigging.¹⁰

In the phantom, only small differences were found between validation T_1 times and our model, but T_1 estimation has limitations. The inversion efficiency is not included in the signal model. It was shown in previous studies that this leads to T_1 underestimation of up to 5%, depending on the type of inversion pulse and relaxation times.^{9,33} This will affect T_1^{moco} as well as the IR-SE validation experiment. Because expected errors are in the range of the SD of T_1 errors in the phantom experiment and the inversion efficiency depends on T_1 as well as T_2 , the inversion efficiency is not considered in this study. Furthermore, through-plane motion occurs during the systolic phase of the cardiac cycle, which is not considered in the signal model for continuous acquisition¹ used for T_1 fitting. Also, the slice profile is not explicitly considered in the model, which could lead to underestimation of T_1 ,³⁴ but its impact is assumed to be small for small flip angles used in our method. Both through-plane motion and slice profile

could cause an estimated effective flip angle that is smaller compared to the nominal flip angle (Supporting Information Figure S2). Further investigation has to be performed on the influence of inversion efficiency, through-plane motion, and the slice profile on T_1 accuracy. The time between inversions was fixed to 2276 ms for simplicity, which was optimized in a previous study for 1 cardiac phase.²⁴ A different time or varying intervals would also possibly work due to the dense sampling by using more TI images. For analysis, we have not carried out a blinded review of the image quality between uncorrected and corrected T_1 maps.

Estimated cardiac contraction during systole was 4.51 ± 0.98 mm averaged over the whole myocardium of the left ventricle, which is in the range of published deformations of the left ventricle (4.6 to 5.5 mm in a midventricular section).³⁵ Small differences between repeated motion estimations ($0.25 \text{ mm} \pm 0.17 \text{ mm}$) suggest reproducibility of the estimation. However, accuracy of the motion estimation cannot be evaluated with this experiment because no independent reference was used. Future research should therefore focus on obtaining cardiac motion estimation using, for example, tissue phase mapping or tagging^{36,37} as independent reference measures.

Motion estimation with this technique is not only restricted to cine images obtained in short axis orientation; motion-corrected T_1 mapping was also successfully carried out in a 4-chamber view. Here, especially visualization of the lateral wall was strongly improved using motion correction, which can be seen by more homogeneous T_1 times in the lateral wall than in T_1 mapping without motion correction. In addition, different software or techniques could be used for motion estimation in the future. For example, feature tracking could be implemented, which seems promising for the detection of cardiac motion.³⁸ However, the myocardium has to be contoured in this approach, which is not the case in NiftyReg. So far, motion transformation is performed in image space requiring interpolation, which could lead to partial volume effects and residual blurring of image data. Nevertheless, cardiac motion correction could possibly be integrated in TI image reconstruction to further increase sharpness of the anatomy by iteratively optimizing image quality.¹¹

Cine images with and without contrast agent administration showed constant contrast over all 12 cardiac phases, although the contrast changed during magnetization recovery (Figures 3 and 4) (Supporting Information Video S1 and S2). The radial data acquisition ensures that combining raw data with different image contrasts leads to a high image quality with only small artifacts due to the inconsistencies in k-space caused by the contrast change. Compared to standard cine imaging, complementary contrast was obtained due to dependencies of T_1 instead of the inflow of blood.

In this study, motion was estimated in 2D; however, the motion estimation algorithm can also be used for a 3D acquisition. This could be beneficial for structures with a high

degree of through-plane motion, such as the papillary muscles and basal segments of the heart.³⁵ Therefore, a 3D acquisition could improve to detect complex cardiac motion. It could also help to reduce the scan time of a 3D T_1 mapping acquisition by improving the scan efficiency compared to proposed 3D T_1 mapping techniques^{39,40} and eventually allow for T_1 mapping of the entire heart in a clinically feasible scan time. Respiratory motion also would have to be accounted for because a 3D acquisition would be too long for a breath-hold. For that, a rigid motion correction could possibly be integrated for which the k-space center could serve as navigator signal. Using a 3D acquisition, through-plane motion could be detected, and systolic cardiac phases would not have to be excluded, which would further increase scan efficiency.

TI images were reconstructed with iterative SENSE, without spatial or temporal filtering of the data. These images have severe streaking artifacts. Other advanced reconstruction techniques could have also been applied, such as compressed sensing, model-based reconstruction, low-rank methods, or integration of motion-compensation in image reconstruction to further improve image quality.^{11,31,41-43}

Postcontrast T_1 maps were in good agreement with LGE images in subjects with focal fibrosis in midventricular and basal SAX. In future research, the approach should be evaluated in a larger patient cohort, especially in patients with irregular or more complex heart motion.

In only 8 s, a $1.3 \times 1.3 \text{ mm}^2$ image resolution was achieved. This short scan duration has the potential for the acquisition of 2 slices within a single breath-hold, which would allow for the number of breath-holds to be reduced in the clinical routine. In addition, the image resolution could possibly also be further increased by prolonging the scan to a breath-hold duration of 10 to 16 s, which is still feasible in patients.

5 | CONCLUSION

In this study, native and postcontrast cardiac T_1 mapping with in-plane resolution of $1.3 \times 1.3 \text{ mm}^2$ obtained in an 8 s breath-hold was shown. Continuous data acquisition and the integration of cardiac motion correction improved the data acquisition efficiency by a factor of 5 compared to standard triggered cardiac T_1 mapping techniques. This increased efficiency resulted in more precise T_1 maps (40% lower SD in the myocardium). Accurate detection of focal fibrosis in postcontrast T_1 maps was feasible using this technique.

ACKNOWLEDGMENT

The authors acknowledge the cofunding and support of the work by the German Research Foundation (DFG-RTG2260 BioQic, DFG-CRC1340 Matrix in Vision).

ORCID

Kirsten M. Becker  <https://orcid.org/0000-0002-8165-5943>

Christoph Kolbitsch  <https://orcid.org/0000-0002-4355-8368>

REFERENCES

- Radenkovic D, Weingärtner S, Ricketts L, Moon JC, Captur G. T1 mapping in cardiac MRI. *Heart Fail Rev*. 2017;22:415–430.
- Kramer CM. Role of cardiac MR imaging in cardiomyopathies. *J Nucl Med*. 2015;56:39S–45S.
- Von Knobelsdorff-Brenkenhoff F, Schulz-Menger J. Cardiovascular magnetic resonance imaging in ischemic heart disease. *J Magn Reson Imaging*. 2012;36:20–38.
- Kali A, Choi E-Y, Sharif B, et al. Native T1 mapping by 3-T CMR imaging for characterization of chronic myocardial infarctions. *JACC Cardiovasc Imaging*. 2015;8:1019–1030.
- Małek ŁA, Werys K, Kłopotowski M, et al. Native T1-mapping for non-contrast assessment of myocardial fibrosis in patients with hypertrophic cardiomyopathy: comparison with late enhancement quantification. *Magn Reson Imaging*. 2015;33:718–724.
- Wong TC, Piehler K, Meier CG, et al. Association between extracellular matrix expansion quantified by cardiovascular magnetic resonance and short term mortality. *Circulation*. 2012;126:1206–1216.
- Messroghli DR, Radjenovic A, Kozerke S, Higgins DM, Sivananthan MU, Ridgway JP. Modified look-locker inversion recovery (MOLLI) for high-resolution T1 mapping of the heart. *Magn Reson Med*. 2004;52:141–146.
- Chow K, Flewitt JA, Green JD, Pagano JJ, Friedrich MG, Thompson RB. Saturation recovery single-shot acquisition (SASHA) for myocardial T1 mapping. *Magn Reson Med*. 2014;71:2082–2095.
- Kellman P, Hansen MS. T1-mapping in the heart: accuracy and precision. *J Cardiovasc Magn Reson*. 2014;16:2.
- Meßner NM, Budjan J, Loßnitzer D, et al. Saturation-recovery myocardial T1-mapping during systole: accurate and robust quantification in the presence of arrhythmia. *Sci Rep*. 2018;8:5251.
- Pang J, Chen Y, Fan Z, et al. High efficiency coronary MR angiography with nonrigid cardiac motion correction. *Magn Reson Med*. 2016;76:1345–1353.
- Kolbitsch C, Ahlman MA, Davies-Venn C, et al. Cardiac and respiratory motion correction for simultaneous cardiac PET/MR. *J Nucl Med*. 2017;58:846–852.
- Roujol S, Foppa M, Weingärtner S, Manning WJ, Nezafat R. Adaptive registration of varying contrast-weighted images for improved tissue characterization (ARCTIC): application to T1 mapping. *Magn Reson Med*. 2015;73:1469–2582.
- Roujol S, Basha TA, Weingärtner S, et al. Impact of motion correction on reproducibility and spatial variability of quantitative myocardial T2 mapping. *J Cardiovasc Magn Reson*. 2015;17:46.
- Xue H, Shah S, Greiser A, et al. Motion correction for myocardial T1 mapping using image registration with synthetic image estimation. *Magn Reson Med*. 2012;67:1644–1655.
- Zhu Y, Kang J, Duan C, et al. Integrated motion correction and dictionary learning for free-breathing myocardial T1 mapping. *Magn Reson Med*. 2019;81:2644–2654.
- Mehta BB, Chen X, Bilchick KC, Salerno M, Epstein FH. Accelerated and navigator-gated look-locker imaging for cardiac T1 estimation (ANGIE): development and application to T1 mapping of the right ventricle. *Magn Reson Med*. 2014;160:150–160.
- Weingärtner S, Roujol S, Akçakaya M, Basha TA, Nezafat R. Free-breathing multislice native myocardial T1 mapping using the slice-interleaved T1 (STONE) sequence. *Magn Reson Med*. 2015;74:115–124.
- Winkelmann S, Schaeffter T, Koehler T, Eggers H, Doessel O. An optimal radial profile order based on the golden ratio for time-resolved MRI. *IEEE Trans Med Imaging*. 2007;26:68–76.
- Block KT, Uecker M, Frahm J. Undersampled radial MRI with multiple coils. Iterative image reconstruction using a total variation constraint. *Magn Reson Med*. 2007;57:1086–1098.
- Rueckert D, Sonoda LI, Hayes C, Hill D, Leach MO, Hawkes DJ. Nonrigid registration using free-form deformations: application to breast MR images. *IEEE Trans Med Imaging*. 1999;18:712–721.
- Modat M, McClelland J, Ourselin S. Lung registration using the NiftyReg package. In Proceedings of the Medical Image Analysis for the Clinic: A Grand Challenge, Workshop from MICCAI 2010, Beijing, China, 2010. p. 33–42.
- Deichmann R, Haase A. Quantification of T1 Values by SNAPSHOT-FLASH NMR Imaging. *J Magn Reson*. 1992;96:608–612.
- Becker KM, Schulz-Menger J, Schaeffter T, Kolbitsch C. Simultaneous high-resolution cardiac T1 mapping and cine imaging using model-based iterative image reconstruction. *Magn Reson Med*. 2019;81:1080–1091.
- Pruessmann KP, Weiger M, Scheidegger MB, Boesiger P. SENSE: sensitivity encoding for fast MRI. *Magn Reson Med*. 1999;42:952–962.
- Captur G, Gatehouse P, Keenan KE, et al. A medical device-grade T1 and ECV phantom for global T1 mapping quality assurance: the T1 mapping and ECV standardization in cardiovascular magnetic resonance (TIMES) program. *J Cardiovasc Magn Reson*. 2016;18:58.
- Cerqueira MD, Weissman NJ, Dilsizian V, et al. Standardized myocardial segmentation and nomenclature for tomographic imaging of the heart: a statement for healthcare professionals from the cardiac imaging. *Circulation*. 2002;105:539–542.
- Ehse P, Seiberlich N, Ma D, et al. IR TrueFISP with a golden-ratio-based radial readout: fast quantification of T1, T2, and proton density. *Magn Reson Med*. 2013;69:71–81.
- Piechnik SK, Ferreira VM, Lewandowski AJ, et al. Normal variation of magnetic resonance T1 relaxation times in the human population at 1.5 T using ShMOLLI. *J Cardiovasc Magn Reson*. 2013;15:13.
- von Knobelsdorff-Brenkenhoff F, Prothmann M, Dieringer MA, et al. Myocardial T1 and T2 mapping at 3 T: reference values, influencing factors and implications. *J Cardiovasc Magn Reson*. 2013;15:53.
- Christodoulou AG, Shaw JL, Nguyen C, et al. Magnetic resonance multitasking for motion-resolved quantitative cardiovascular imaging. *Nat Biomed Eng*. 2018;2:215–226.
- Weingärtner S, Meßner NM, Budjan J, et al. Myocardial T1-mapping at 3T using saturation-recovery: reference values, precision and comparison with MOLLI. *J Cardiovasc Magn Reson*. 2016;18:84.
- Kellman P, Herzka DA, Schacht HM. Adiabatic inversion pulses for myocardial T1-mapping. *Magn Reson Med*. 2014;71:1428–1434.
- Cooper MA, Nguyen TD, Spincemaille P, Prince MR, Weinsaft JW, Wang Y. Flip angle profile correction for T1 and T2 quantification with look-locker inversion recovery 2D steady-state free precession imaging. *Magn Reson Med*. 2012;68:1579–1585.

35. Scott AD, Keegan J, Firmin DN. Motion in cardiovascular MR imaging. *Radiology*. 2009;250:331–351.
36. Pelc LR, Sayre J, Yun K, et al. Evaluation of myocardial motion tracking with cine-phase contrast magnetic resonance imaging. *Invest Radiol*. 1994;29:1038–1042.
37. Zerhouni EA, Parish DM, Rogers WJ, Yang A, Shapiro EP. Human heart: tagging with MR imaging: a method for noninvasive assessment of myocardial motion. *Radiology*. 1988;169:59–63.
38. Cao JJ, Ngai N, Duncanson L, Cheng J, Gliganic K, Chen Q. A comparison of both DENSE and feature tracking techniques with tagging for the cardiovascular magnetic resonance assessment of myocardial strain. *J Cardiovasc Magn Reson*. 2018;20:26.
39. Nordio G, Henningsson M, Chiribiri A, Villa A, Schneider T. 3D Myocardial T₁ mapping using saturation recovery. *J Magn Reson Imaging*. 2017;46:218–227.
40. Shaw J, Christodoulou A, Bi X, Li D. 3D whole-ventricle, free-breathing, non-ECG, myocardial T₁ and ECV mapping with CMR multitasking. In Proceedings of the 26th Annual Meeting of ISMRM, Paris, France, 2018, Abstract 4872.
41. Lustig M, Donoho D, Pauly JM. Sparse MRI: the application of compressed sensing for rapid MR imaging. *Magn Reson Med*. 2007;58:1182–1195.
42. Tran-Gia J, Wech T, Bley T, Köstler H. Model-based acceleration of look-locker T₁ mapping. *PLoS ONE*. 2015;10:e0122611.
43. Kolda TG, Bader BW. Tensor decompositions and applications. *SIAM Rev*. 2009;51:455–500.

SUPPORTING INFORMATION

Additional supporting information may be found online in the Supporting Information section at the end of the article.

FIGURE S1 Phantom evaluation. T₁ times showed good correlation with the reference IR-SE T₁ times ($R^2 > 0.99$). Differences were $0.28\% \pm 3.70\%$ over all 9 vials

FIGURE S2 Maps of all estimated parameters. The estimated effective flip angle was smaller in myocardium (around 4°) compared to the nominal flip angle (5°). This could be caused by an imperfect slice profile, B₁ inhomogeneity and through-plane motion of the heart during systole. In blood, the effective flip angle was smaller compared to myocardium, possibly because of compensation for inflow effects of spins which have not experienced RF pulses before

VIDEO S1 Cine images and motion correction without contrast administration. The deformation of the heart was estimated and motion was corrected (right) to match the reference mid-diastolic phase. Three systolic cardiac phases were excluded. The temporal slice profiles of cine images with and without motion correction are shown in the lower row (red line)

VIDEO S2 Cine images and motion correction after contrast administration. The deformation of the heart was estimated and motion was corrected (right) to match the reference mid-diastolic phase. Three systolic cardiac phases were excluded. The temporal slice profiles of cine images with and without motion correction are shown in the lower row (red line)

VIDEO S3 Cine images and estimated cardiac motion fields. Here all 15 cardiac phases are shown, overlaid by its motion field, which was used to correct for motion in T₁ mapping

How to cite this article: Becker KM, Blaszczyk E, Funk S, et al. Fast myocardial T₁ mapping using cardiac motion correction. *Magn Reson Med*. 2020;83:438–451. <https://doi.org/10.1002/mrm.27935>